Orientation Independence of Single-Vacancy and Single-Ion Permeability Ratios

Pete McGill and Mark F. Schumaker
Department of Pure and Applied Mathematics, Washington State University, Pullman, Washington 99164 USA

ABSTRACT Single-vacancy models have been proposed as open channel permeation mechanisms for K^+ channels. Single-ion models have been used to describe permeation through Na^+ channels. This paper demonstrates that these models have a distinctive symmetry property. Their permeability ratios, measured under biionic conditions, are independent of channel orientation when the reversal potential is zero. This symmetry is a property of general m-site single-vacancy channels, m-site shaking-stack channels, as well as m-site single-ion channels. An experimental finding that the permeability ratios of a channel did not have this symmetry would provide evidence that a single-vacancy or single-ion model is an incorrect or incomplete description of permeation.

INTRODUCTION

Single-vacancy models have been used successfully to describe the open-channel permeation properties of several K^+ channels (Schumaker and MacKinnon, 1990; Clay, 1991; Schumaker, 1992; Lu and MacKinnon, 1994). Beginning with the work of Hodgkin and Keynes (1955), certain K^+ channels have been suspected to have multi-ion pores. Hille (1992) provides an extensive review. Recent experimental evidence suggests that several high affinity cation binding sites line the permeation pore of K^+ channels. Vestergaard-Bogind et al. (1985) measured the flux ratio exponent of the Gardos K^+ channel in human red blood cells. They found an exponent of $\sim$2.7 over a range of internal and external cation concentrations and transmembrane potentials, suggesting that three or more K^+ ions occupy the pore. Neyton and Miller (1988a,b) studied the escape of Ba^{2+} ions trapped in the pore of the high-conductance Ca^{2+}-activated K^+ (CaK) channel and concluded that four cation binding sites line the pore, with at least three occupied under normal physiological conditions. Motivated by these experiments, Schumaker and MacKinnon (1990) proposed a single-vacancy mechanism to model permeation through these channels: a pore with m ion binding sites occupied by at least $m - 1$ cations. This simple case of discrete state models had been studied previously by Kohler and Heckmann (1979) and Levitt (1984). Schumaker (1992) subsequently introduced the shaking-stack model, a variant of the single-vacancy mechanism, as an explanation for the seemingly paradoxical combination of high conductance and selectivity seen in the CaK channel (Eisenman et al., 1986).

Our knowledge of the structure of the K^+ channel permeation pore does not exclude the single-vacancy permeation mechanism. Based in part on the mutation experiments of Heginbotham et al. (1994), Guy and Durrell (1994) have developed a series of models for the P region of the K^+ channel pore in which the narrowest part has backbone carbonyl oxygens projecting inward into the pore. In one of these models, five tetrads of oxygens form four or five similar regions where cations might plausibly bind. This proposed structure could conceivably support the closely spaced high affinity binding sites envisioned in the shaking-stack model.

Despite the successes of the single-vacancy model, it is certainly an oversimplification of the open channel permeation process through the complex structure of an actual ion channel. As one example of simplification, the discrete state formalism of these models can be justified only by special physical circumstances. Several authors (Cooper et al., 1985, 1988; Dani and Levitt, 1990) have emphasized that these models assume that an ion achieves a local equilibrium at a potential energy minimum before making a rapid transition over a neighboring energy barrier. These conditions require well localized binding sites, with neighboring barriers of at least 4 or 5 k_BT (k_B denotes Boltzmann's constant and T absolute temperature). Furthermore, models that are qualitatively different from the single-vacancy mechanisms may be able to interpret the same kinetic data. Bek and Jakobsson (1994) have shown that several general features of K^+ channel conduction can be reproduced by a multi-ion model in which transport takes place by diffusion along a flat potential energy trough characterized only by its partition energy with respect to the bathing solutions.

Na^+ channels have been modeled by both single-ion and three-barrier two-site (3B2S) double-occupancy theories. Ravindran et al. (1992) and Naranjo and Latorre (1993) provide good discussions of both modeling approaches. Our investigation was motivated, in part, by experiments on the orientation dependence of the reversal potential in the Na^+ channel (Begenisich and Cahalan, 1980; Garber, 1988).

Received for publication 3 November 1994 and in final form 3 April 1995.
Address reprint requests to Dr. Mark F. Schumaker, Department of Pure and Applied Mathematics, Washington State University, Pullman, WA 99164–3113. Tel.: 509-335-3170; Fax: 509-335-1188; E-mail: schumaker@beta.math.wsu.edu.

0006-3495/95/07/84/10 $2.00

Garber measured the reversal potentials of single Na^+ channels in planar lipid bilayers and found that the biionic Na^+/K^+ permeability ratio depended on the orientation of the permeant ions with respect to the internal and external faces of the channel. More recently, the orientation dependence of K^+ channel reversal potentials has also been measured (Heginbotham and MacKinnon, 1993; Pérez-Cornejo and Begenisich, 1994). The major result of this paper is that the biionic permeability ratios of single-vacancy and single-ion models must be independent of channel orientation at zero applied transmembrane potential. This result could provide a way to falsify these models.

ORIENTATION INDEPENDENCE OF THE REVERSAL POTENTIAL

Fig. 1, *A* and *B*, sketch channels embedded in a membrane between two cups of electrolyte. We refer to the cup on the left as side 1 and the cup on the right as side 2. The channels have a definite orientation with respect to the cups, for example, the intracellular end of the channel on side 1. This fixed orientation is suggested by the arrows in the figure. The surrounding solutions contain two permeant cations, X and Y, under biionic conditions. In Fig. 1*A*, the solution on side 1 contains the ion X but no significant amount of Y, and the solution on side 2 contains Y but no significant X. We refer to this as the orientation $[X \,\|\, Y]$ of the solutions. The activity of ion X on side 1 by is denoted by x_1 and the activity of Y on side 2 by y_2 (subscripts on ion activities will not always indicate sides). We refer to the orientation of the ions and their activities together as their configuration, denoted in this case by the symbol $[x_1 \,\|\, y_2]$. The reversal potential is the applied transmembrane electrical potential that results in zero net current through the channel. Its value in the configuration $[x_1 \,\|\, y_2]$ will be denoted $V_R(x_1, y_2)$. In Fig. 1*B* the orientation of permeant ions is reversed, with configuration $[y_1 \,\|\, x_2]$ and reversal potential $V_R(y_1, x_2)$.

Suppose that the conductance properties of the channel in Fig. 1 were symmetrical and that $x_1 = x_2 = x_0$ and $y_1 = y_2 = y_0$. Then the ion currents corresponding to Fig. 1*B* would be the mirror image of those corresponding to Fig. 1*A*. The corresponding reversal potentials would have the same magnitude:

$$V_R(x_0, y_0) = -V_R(y_0, x_0), \tag{1}$$

with the minus sign arising from the fixed orientation of the electrodes. In general, we say that the reversal potential is orientation independent whenever Eq. 1 is satisfied. This may occur even when channel conduction properties are not fully symmetrical.

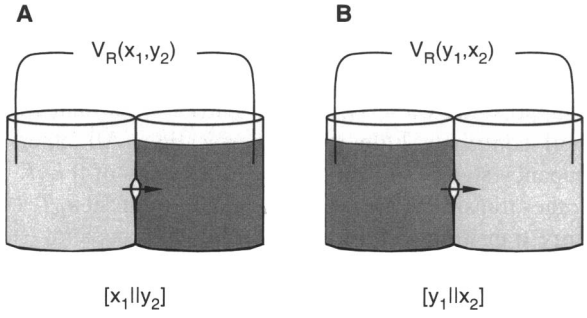

FIGURE 1 Hypothetical reversal potential measurements in the biionic orientations $[X \,\|\, Y]$ and $[Y \,\|\, X]$. Arrows indicate the fixed orientation of the channels with respect to cup 1 (on the left) and cup 2. (*A*) Configuration $[x_1 \,\|\, y_2]$. The activity of cation X in cup 1 is x_1, and the activity of Y is negligible. The activity of cation Y in cup 2 is y_2, and the activity of X is negligible. The reversal potential is denoted $V_R(x_1, y_2)$, with the convention that the potential on side 2 is zero. (*B*) Configuration $[y_1 \,\|\, x_2]$.

Fig. 2, *A* and *B*, shows reversal potential symmetry plots, a way to graph reversal potentials that makes manifest the presence or absence of the orientation independence symmetry over a range of reversal potentials. For each of the model permeation mechanisms discussed below, reversal potentials are calculated for the configurations $[x_0 \,\|\, y_i]$ and $[y_i \,\|\, x_0]$, where x_0 is held constant while several values of y_i are considered. As y_i increases, $V_R(x_0, y_i)$ increases and $V_R(y_i, x_0)$ decreases, so that the symmetry plot progresses from the second to the fourth quadrant. The graphs are constructed by drawing a curve through several ordered pairs $(V_R(x_0, y_i), V_R(y_i, x_0))$. The concentrations x_0 and y_i do not appear explicitly in the graphs but parameterize the curves. The orientation independence symmetry, Eq. 2, corresponds to the solid line shown in Fig. 2*A*, which passes through the origin with slope -1. Symmetry plots for symmetric ion transport mechanisms must fall on this line.

Reversal potentials are closely related to the idea of permeability ratio (Hille, 1992). The ratio of Y ion permeability to X ion permeability is often denoted P_Y/P_X. However, we will introduce a notation to distinguish between the value of this quantity in the configurations $[x_0 \,\|\, y_0]$ and $[y_0 \,\|\, x_0]$:

$$r(x_0, y_0) = \frac{P_Y}{P_X}\bigg|_{[x_0\|y_0]} = \frac{x_0}{y_0} \exp \frac{zeV_R(x_0, y_0)}{k_B T}. \tag{2}$$

$$r(y_0, x_0) = \frac{P_Y}{P_X}\bigg|_{[y_0\|x_0]} = \frac{x_0}{y_0} \exp \frac{-zeV_R(y_0, x_0)}{k_B T}. \tag{3}$$

When Eq. 3 is satisfied, we see that permeability ratios are also independent of orientation. The ratio of $r(x_0, y_0)$ and $r(y_0, x_0)$ is given by:

$$\frac{r(x_0, y_0)}{r(y_0, x_0)} = \exp \frac{ze}{k_B T}[V_R(x_0, y_0) + V_R(y_0, x_0)]. \tag{4}$$

The ratio on the left hand side is greater than 1 if and only if the sum of the reversal potentials on the right is greater than 0. In other words, the region above the solid line in Fig. 2*A* corresponds to the case that the permeability ratio P_Y/P_X is greater in configuration $[x_0 \,\|\, y_0]$ than in configuration $[y_0 \,\|\, x_0]$.

The main result of this paper is that reversal potential symmetry plots for single-ion and single-vacancy (including shaking-stack) transport mechanisms must intersect the origin of the symmetry plot. That is, their reversal potentials

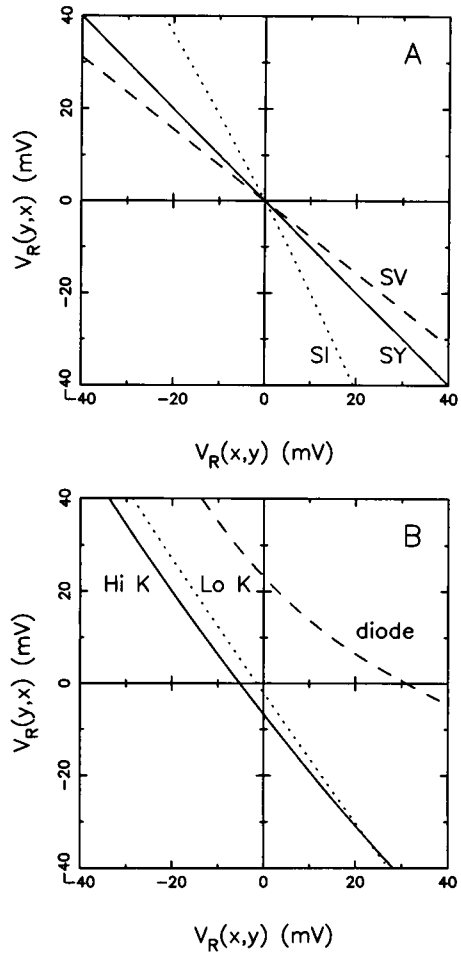

FIGURE 2 Reversal potential symmetry plots for several model permeation mechanisms. (*A*) Three examples that have the orientation independence symmetry at $V_R = 0$. All symmetric ion transport mechanisms give the plot SY. SV and SI are examples of single-vacancy and single-ion symmetry plots, respectively. The central result of this paper is that symmetry plots for these mechanisms must pass through the origin. Single-ion example occupancy state energies, in k_BT, are as follows: $G(2) = G(3) = 3$; $G(5) = G(7) = 0$; $G(8) = -2$. Single-ion transition state energies: $G(2, 3) = 10$; $G(2, 5) = G(3, 5) = G(5, 7) = 11$; $G(5, 8) = G(7, 8) = 7$. Single-vacancy example occupancy state energies: $G(1) = G(4) = G(6) = G(7) = G(8) = G(9) = 0$; $G(2) = 2$; $G(3) = 4$. Single-vacancy example transition state energies: $G(1, 2) = G(2, 3) = G(2, 4) = G(3, 6) = G(4, 7) = G(6, 8) = 10$; $G(1, 3) = 8$; $G(7, 8) = G(7, 9) = 9$; $G(8, 9) = 7$. State numbers refer to the 3B2S diagrams shown in Fig. 3. (*B*) Three examples showing violations of the orientation independence symmetry at $V_R = 0$. The diode example demonstrates large violations of this symmetry; its construction is described in Fig. 3, *A* and *B*, and the text. The other two curves are generated from the 3B2S double-occupancy model for a Na^+ channel proposed by Ravindran et al. (1992). In the Hi K example, $[K^+] = 1.15$ M activity and 40 mM $< [Na^+] <$ 670 mM. In the Lo K example $[K^+] = 77$ mM activity and 3 mM $< [Na^+] <$ 40 mM. An inter-ion repulsion factor is also used, as described in the legend of Fig. 3. Na^+ and K^+ potential energy profiles for this model are shown in Fig. 3*C*.

(or permeability ratios) are orientation independent when $V_R = 0$. Our proof does not depend on the specific values of parameters in these models; the result is a qualitative feature of these conduction mechanisms.

The dotted and dashed curves in Fig. 2*A* give examples of symmetry plots for single-vacancy and single-ion mechanisms. Their slopes differ significantly from -1 near the origin, implying that $V_R(x, y)$ and $V_R(y, x)$ have a different dependence on activity ratios. In particular, the dependence of the reversal potential on the activity ratio for at least one of the orientations must deviate significantly from the Nernstian 56 mV per decade. Such a deviation was observed by Begenisich and Cahalan (1980) in their measurements of Na^+ channel Na^+/NH_4^+ reversal potentials in voltage-clamped squid axons. In contrast to the cases shown in Fig. 2*A*, one can also find examples of highly asymmetrical single-ion and single-vacancy conduction mechanisms whose reversal potentials are very nearly consistent with Eq. 1 over a wide range of concentrations.

For convenience, all of the examples shown in Fig. 2, *A* and *B*, were constructed by using absolute rate theory expressions for rate constants (e.g., Glasstone et al., 1941). The rate for transitions from state i to state j is given by $k(i, j) = \kappa \exp -[G(i, j) - G(i)]/k_BT$, where $\kappa = 6.11 \times 10^{12}$ s^{-1}, $G(i)$ is the free energy (per channel) for occupancy state i and $G(i, j)$ is the height of the free energy barrier between states i and j. Values of $G(i)$ and $G(i, j)$ for the single-vacancy and single-ion examples are given in the legend of Fig. 2. Rates for transitions $k(i, j)$ in the direction of an applied transmembrane field V are multiplied by a factor of $\exp(\alpha_{ij}eV/k_BT)$, and rates for transitions against the field are multiplied by $\exp(-\alpha_{ij}eV/k_BT)$. In these factors, the α_{ij} values are the electrical distances associated with each transition. They have a value of $\alpha_{ij} = 1/6$, except for the Na^+ channel model discussed below. Ion valences are $+1$.

We next give an example of a three-barrier two-site (3B2S) double-occupancy transport mechanism that shows how permeability ratios can depend strongly on orientation. 3B2S state diagrams for the orientations $[X \| Y]$ and $[Y \| X]$ are given by Fig. 3, *A* and *B*, respectively. Directed transitions between occupancy states are indicated by arrowheads. Reverse transitions are impossible because of the biionic conditions. All other transitions are bidirectional. The only asymmetry between the permeation properties of X and Y is the suppression of the 2–5 transition rate by a high 15 k_BT barrier. We also assume that states 1 and 9 are high energy (5 k_BT) and that transitions to these latter states are suppressed by a 15 k_BT energy barrier. Then states 1 and 9 will contribute little to ion permeation. All other ion occupancy states are then assigned an energy of 0 k_BT, and all other transitions are assigned an energy of 10 k_BT. High energy transition states and high energy occupancy states are indicated by asterisks in Fig. 3. The phrase suppressed transition will refer to transitions over high energy barriers.

The symmetry plot for this model is shown in Fig. 2*B*, labeled diode. It was constructed by setting $x_0 = 1M$, and varying 10 mM $< y_0 <$ 250 mM. The path of the curve, and the discussion of Eq. 5, imply a strong orientation dependence of the permeability ratio: $r(x_0, y_0) \gg r(y_0, x_0)$. This result can be understood by analyzing the state diagrams in

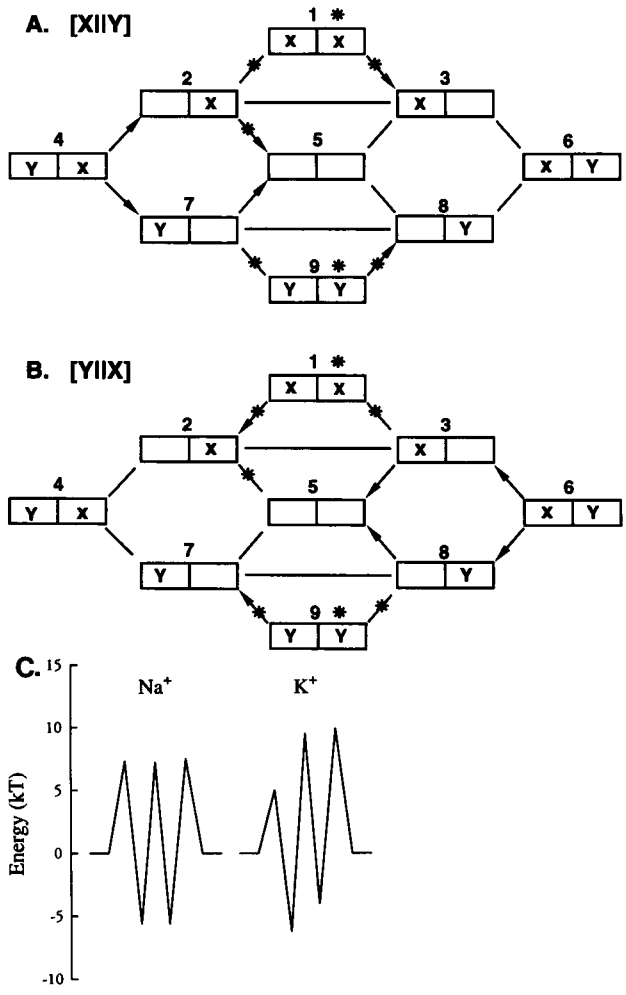

FIGURE 3 Construction of examples violating the orientation independence symmetry at $V_R = 0$. (*A*) Diode example in the orientation $[X \| Y]$. Directed transitions between occupancy states are shown by arrowheads, all other transitions are bidirectional. All occupancy states are assigned an energy of 0 k_BT, except states 1 and 9 (asterisks), which are assigned energies of 5 k_BT. All transition states energies are 10 k_BT, except those marked by asterisks, which are 15 k_BT. (*B*) Diode model in the orientation $[Y \| X]$. (*C*) Potential energy profiles for Na^+ and K^+ in the 3B2S double-occupancy Na^+ channel model of Ravindran et al. (1992). Energies shown correspond to a 1 M solution reference state. Na^+ barrier energies are (left to right, in units of k_BT) 7.31, 7.24, and 7.52; well energies are −5.59 and −5.62. K^+ barrier energies are 5.02, 9.49, and 9.95; well energies are −6.21 and −4.01. For both ions, fractional electrical distances between the central energy barrier and adjacent wells are 0.15, and all others are 0.175. Ion energies in the doubly occupied state are increased by the repulsion factor A/d, where $A = 2.16\ k_BT$ and d is the fractional electrical distance between the ions.

Fig. 3. Consider the configuration $[x_1 \| y_2]$, corresponding to Fig. 3*A*. *Y* ions permeate freely from side 2 to side 1 via the cycles 5–8–7 and 5–3–6–8-7. However, there are no cycles available to transport *X* ions from side 1 to side 2 that do not involve suppressed transitions. As a result, the permeability ratio $r(x_1, y_2) \gg 1$ and grows without bound as the height of the energy barriers associated with the suppressed transitions increase (hence the label diode). Now consider the configuration $[y_1 \| x_2]$, Fig. 3*B*. *Y* ions can permeate from side 1 to side 2 via the cycle 5–7–8, and *X* ions can permeate in the reverse direction via the cycle 5–7–4–2–3, which does not involve suppressed transitions. These cycles remain active as the height of the energy barriers associated with the suppressed transitions increases and the permeability ratio $r(y_1, x_2)$ approaches a finite limit. (The example can be understood in terms of this limiting argument in part because of the high fixed value of $[x_0]$ = 1 M. For smaller $[x_0]$, the limiting regime described above is encountered only when the energy barriers associated with the suppressed transitions are higher.)

The second example showing violation of the orientation independence symmetry at $V_R = 0$ is the 3B2S double-occupancy model of Ravindran et al. (1992) for the rat skeletal Na^+ channel. The symmetry plots are labeled Hi K and Lo K in Fig. 2*B*. In both cases, K^+ is identified with X^+ and Na^+ with Y^+. To construct the high $[K^+]$ curve, we fixed $[K^+]$ = 1.15 M activity (corresponding to a 2 molal solution). To construct the low $[K^+]$ curve, we fixed $[K^+]$ = 77 mM activity (0.1 molal). In both cases, $[Na^+]$ was varied over a suitable range of values. Fig. 3*C* shows free energy profiles for these ions; that of Na^+ is nearly symmetrical whereas that of K^+ is highly asymmetrical. This Na^+ channel model also includes an inter-ion repulsion factor of the form A/d, where A is a constant and d is the fractional electrical distance between ions in a given occupancy or transition state. The repulsion factors specified for this model do not depend on the ion species. All parameter values are given in the legend of Fig. 3.

The low $[K^+]$ example shows only a small violation of the orientation independence symmetry near $V_R = 0$. The symmetry plot intersects the axes at (−1.5 *mV*, 0 *mV*) and (0 *mV*, −2.1 *mV*) In this regime, the 3B2S model of Ravindran et al. has a 16% probability of being empty and an 84% probability of being singly occupied but only a 0.1% probability of being doubly occupied. The high $[K^+]$ example shows a more significant violation of the symmetry near $V_R = 0$. The symmetry plot intersects the axes at (−5.2 *mV*, 0 *mV*) and (0 *mV*, −6.6 *mV*). Here, the model has a 1.3% probability of being empty, a 97% probability of being singly occupied, and a 1.7% probability of being doubly occupied.

TWO-SITE SINGLE-VACANCY MODELS HAVE ORIENTATION INDEPENDENCE SYMMETRY AT $V_R = 0$

The central result of this paper is that all single-vacancy and single-ion conduction models satisfy the orientation independence symmetry when $V_R = 0$. In this section we carry the proof out in detail for two-site single-vacancy models. Appendix A obtains the result for two-site single-ion models; the generalization to m sites is straightforward. Appendix B proves the symmetry for m-site single-vacancy models. Appendix C sketches the proof for m-site shaking-stack models. These generalizations are based on the same ideas

as found in the two-site argument below, but the algebraic expressions are more complex when it is necessary to discuss an arbitrary number of ion binding sites.

We begin by introducing our notation for rate constants. Because we are concerned with the orientation independence symmetry at zero transmembrane potential, we do not need to discuss the voltage dependence of these rates. We consider a single-vacancy channel with two binding sites. Site 1 is nearest to the channel entrance at side 1, and site 2 is nearest to the channel entrance at side 2. In the following definitions, Z may stand for either X or Y. The concentration of Z on side 1 of the channel is z_1, and the psuedo-first-order rate constant for an ion to enter from side 1 and bind to a vacant site 1 will be denoted $Z_1 a_Z$. The rate for a second ion, occupying site 2, to exit into the solution on side 2 will be denoted b_Z. The ion on site 1 can then translocate to site 2, and this rate will be denoted c_Z. The corresponding rate constants describing transport from side 2 to side 1 through the channel will be distinguished by primes, $z_2 a'_Z$, b'_Z, and c'_Z. Note that the rate constants a_Z, b_Z, a'_Z, and b'_Z apply only to ion transitions in a channel that has a second binding site occupied by another ion of the same type Z.

Consider briefly the channel conducting current in the presence of a single permeant ion, the configuration $[z_1 \| z_2]$. The net current through the channel will be proportional to the product of rates forward from side 1 to side 2, minus the product of rates backwards from side 2 to side 1 (Schumaker and MacKinnon, 1990). If $z_1 = z_2$ and the transmembrane potential $V = 0$, the system will be at thermodynamic equilibrium, and the net current through the channel must be zero. This leads to the condition for detailed balance

$$a_z b_z c_z = a'_z b'_z c'_z \tag{5}$$

which holds for both $Z = X$ and $Z = Y$.

Now consider the problem of calculating the reversal potential for a two-site single-vacancy channel in the configuration $[x_1 \| y_2]$. The state diagram appears in Fig. 4*A*. An X ion permeates from side 1 to side 2 through the pore every time the cycle 1–2–3 is traversed. Note that the transition from state 3 to state 1 is unidirectional, as we assume $x_2 = 0$ in this configuration. Let $\vec{J}$ denote the

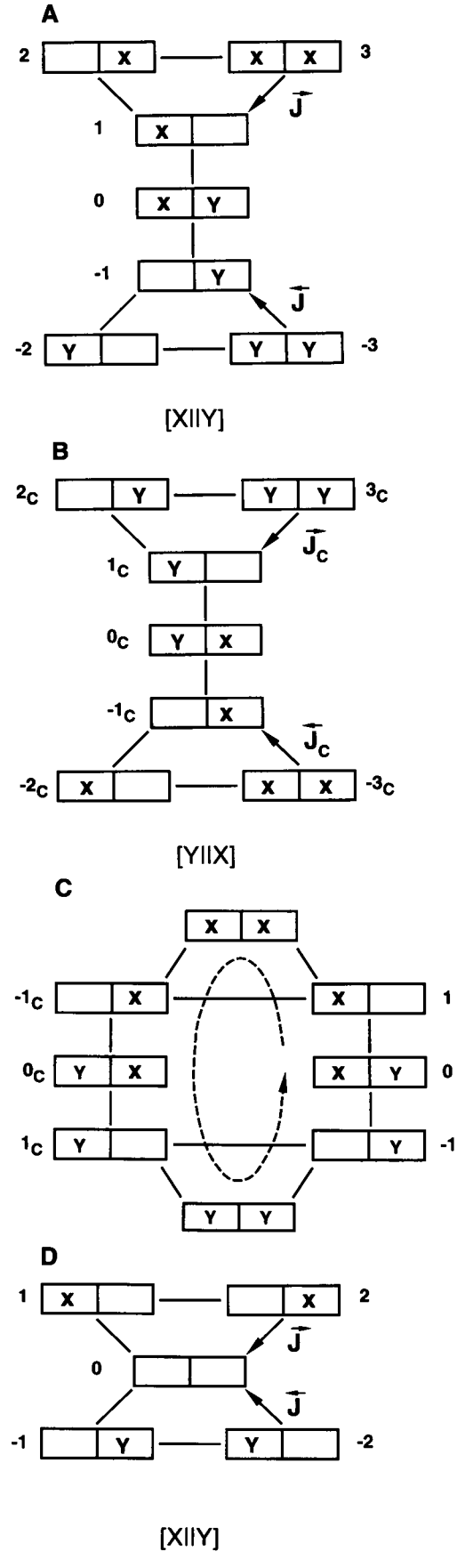

FIGURE 4 (*A*) State diagram for the two-site single-vacancy model in the orientation $[X \| Y]$. All transitions are bidirectional except those denoted by arrows, which are irreversible. The unidirectional flux of X ions from side 1 to side 2, $\vec{J}$, is equal to the flux from state 3 to state 1. The unidirectional flux of Y ions from side 2 to side 1, $\vec{J}$, is equal to the flux from state -3 to state -1. (*B*) State diagram for the two-site single-vacancy model in the orientation $[Y \| X]$. To emphasize the symmetry underlying the transition from Eqs. 14 and 15 in the text, the Y ion occupancy states are shown at top of the diagram and the X ion occupancy states at the bottom. States are relabeled with C (for complementary) subscripts. (*C*) State diagram for the two-site single-vacancy model in the orientation $[X, Y \| X, Y]$. The detailed balance condition for the outermost cycle (*dashed line*) completes the proof of orientation independence at $V_R = 0$. (*D*) State diagram for a two-site single-ion model in the orientation $[X \| Y]$.

unidirectional flux of X ions from side 1 to side 2. According to the King-Altman method (e.g., Hill, 1977), this is given by

$$\vec{J} = D^{-1}A_Y B_{YX} C_X . \tag{6}$$

A_Y is the sum of products of rate constants, corresponding to trees directed out of the bottom cycle of Fig. 4*A*.

$$\begin{aligned} A_Y &= b_Y c_Y + b'_Y c_Y + y_2 a'_Y b'_Y , \\ &= a_Y^{-1}[a_Y b_Y c_Y + a_Y b'_Y c_Y + y_2 a_Y a'_Y b'_Y], \\ &= a_Y^{-1} b'_Y [a'_Y c'_Y + a_Y c_Y + y_2 a_Y a'_Y] . \end{aligned} \tag{7}$$

Detailed balance, Eq. 5, is used to obtain the final expression. B_{YX} is the product of the rate constant up the bridge of states in Fig. 4*A*, connecting the two cycles. We have not defined special symbols for these rates, which involve transitions into or out of states in which the channel is occupied by both ion species. Let $k(i, j)$ denote the first or second order rates from occupancy state i to occupancy state j, where the entrance step is also proportional to x_1:

$$B_{YX} = x_1 k(-1, 0) k(0, 1) . \tag{8}$$

C_X is the product of rate constants clockwise around the top cycle:

$$C_X = x_1 a_X b_X c_X . \tag{9}$$

Finally, D is the denominator common to the formulas for $\vec{J}$ and $\overleftarrow{J}$.

A corresponding set of expressions gives $\overleftarrow{J}$, the unidirectional current of Y ions from side 2 to side 1:

$$\overleftarrow{J} = D^{-1}A_X B_{XY} C_Y , \tag{10}$$

$$A_X = (a'_X)^{-1} b_X [a_X c_X + a'_X c'_X + x_1 a_X a'_X], \tag{11}$$

$$B_{XY} = y_2 k(1, 0) k(0, -1), \tag{12}$$

$$C_Y = y_2 a'_Y b'_Y c'_Y . \tag{13}$$

These formulas can be obtained from Eqs. 6–9 by interchanging X and Y subscripts, primes and nonprimes, and the concentrations x_1 and y_2. We must also replace the product of rate constants up the bridge with the product down the bridge.

The formulas for $\vec{J}$ and $\overleftarrow{J}$ assume that the transmembrane potential is zero. When $\vec{J} = \overleftarrow{J}$, we have the condition for $V_R(x_1, y_2) = 0$:

$$\frac{x_1^2 a_X b_X c_X [a'_Y c'_Y + a_Y c_Y + y_2 a_Y a'_Y]}{y_2^2 a'_Y b'_Y c'_Y [a_X c_X + a'_X c'_X + x_1 a_X a'_X]} = \frac{k(1, 0) k(0, -1)}{k(-1, 0) k(0, 1)} \frac{a_Y b_X}{a'_X b'_Y} . \tag{14}$$

Now consider the channel in the reversed orientation $[y_1 \,\|\, x_2]$, the state diagram of which is shown in Fig. 4*B*. Occupancy states in the reversed orientation will be termed complementary to corresponding states in the original orientation and are denoted by the C subscript. Repeat the derivation given above to obtain the condition for $V_R(y_1, x_2) = 0$:

$$\frac{y_1^2 a_Y b_Y c_Y [a'_X c'_X + a_X c_X + x_2 a_X a'_X]}{x_2^2 a'_X b'_X c'_X [a_Y c_Y + a'_Y c'_Y + y_1 a_Y a'_Y]} = \frac{k(1_C, 0_C) k(0_C, -1_C)}{k(-1_C, 0_C) k(0_C, 1_C)} \frac{a_X b_Y}{a'_Y b'_X} . \tag{15}$$

This formula can be obtained directly from Eq. 14 by interchanging X and Y subscripts and labeling the occupancy states with C subscripts. Take the reciprocal of Eq. 15 and use detailed balance, Eq. 5, to obtain:

$$\frac{x_2^2 a_X b_X c_X [a_Y c_Y + a'_Y c'_Y + y_1 a_Y a'_Y]}{y_1^2 a'_Y b'_Y c'_Y [a'_X c'_X + a_X c_X + x_2 a_X a'_X]} = \frac{k(-1_C, 0_C) k(0_C, 1_C)}{k(1_C, 0_C) k(0_C, -1_C)} \frac{a'_Y b'_X}{a_X b_Y} . \tag{16}$$

Eqs. 14–16 have the respective forms:

$$f(x_1, y_2) = K, \text{ and } f(x_2, y_1) = K_C . \tag{17}$$

where f is the same function on the left side of both equations.

Next show that $K = K_C$. Consider the state diagram for the two-site single-vacancy model in the configuration $[x_0, y_0 \,\|\, x_0, y_0]$, shown in Fig. 4*C*. When the transmembrane potential is zero, this system must be in equilibrium. The detailed balance relationship corresponding to the outermost cycle gives:

$$\begin{aligned} &k(-1, 0) k(0, 1) x_0 a'_X b'_X k(-1_C, 0_C) k(0_C, 1_C) y_0 a'_Y b'_Y \\ &\quad = k(1_C, 0_C) k(0_C, -1_C) x_0 a_X b_X k(1, 0) k(0, -1) y_0 a_Y b_Y . \end{aligned} \tag{18}$$

Rearrange this formula to give $K = K_C$. It follows that Eqs. 14 and 16 are in fact the same. If $x_1 = x_0$ and $y_2 = y_0$ satisfies Eq. 14, which is the condition for $V_R(x_1, y_2) = 0$, then $x_2 = x_0$ and $y_1 = y_0$ satisfies Eq. 16, which is the condition for $V_R(y_1, x_2) = 0$. In other words, the reversal potential for the two-site single-vacancy model is orientation independent when $V_R = 0$. The symmetry plot for the single-vacancy model therefore intersects the origin. This result is independent of the numerical value of model parameters; it is a qualitative property of the single-vacancy conduction model.

DISCUSSION

Single-vacancy and single-ion conduction models have orientation-independent permeability ratios when $V_R = 0$. The proof given above depends only on the discrete state formulation of

these conduction models and the principle of detailed balance. It is interesting that this principle of equilibrium statistical mechanics can be used to demonstrate a model-dependent symmetry under far-from-equilibrium conditions. This symmetry does not depend on the values of model parameters. It also does not depend on how the effects of an applied electrical potential are modeled, as it holds at $V_R = 0$. If the permeability ratios of a real channel failed to observe the orientation independence symmetry, one could conclude that ion conduction did not proceed by a single-ion or single-vacancy mechanism, or at least that other elements were involved.

There are several ways that the single-vacancy model could be incorrect or incomplete, leading to violation of the orientation independence symmetry. The single-vacancy assumption may fail to be satisfied, which could break the symmetry as shown by the examples in Fig. 2*B*. Even if permeation proceeded by a mechanism similar to the single-vacancy model, the symmetry could conceivably be broken by other features of the transport mechanism. As an example, consider asymmetrically distributed surface charges. If reversal potential measurements in both orientations were performed in the presence of such charges, and with significantly different concentrations of two permeant ions at $V_R = 0$ (or with permeant ions having different valence), screening effects would differ in the two orientations. Different electric fields within the channel could then lead to different permeation properties. However, it is interesting to note that the neutralization of surface charges may not change reversal potentials (MacKinnon and Miller, 1989). Allosteric effects could also break the orientation independence symmetry. An allosteric site on one side of the channel could also bind permeant ions with different affinities, giving the channel different permeation properties in the two orientations.

A finding that the orientation independence symmetry is satisfied would not provide definitive evidence in favor of the single-vacancy or single-ion permeation mechanisms. For example, reversal potentials for all symmetric conduction mechanisms must satisfy the orientation independence symmetry at all transmembrane potentials, including $V_R = 0$. However, chemical modification of surface charges or site-directed mutagenesis could conceivably break such symmetry. If the basic mechanism of ion permeation remained the same after the symmetry was broken, single-vacancy or single-ion permeation mechanisms would still give the orientation independence symmetry at $V_R = 0$ (assuming that an additional effect, such as asymmetrical screening, did not break the symmetry).

Diffusion models may also satisfy the orientation independence symmetry. In particular, Levitt's (1986) diffusive single ion theory does, and this result is independent of parameter values. Let the dimensionless transmembrane potential (side 1 − side 2) be defined as $v = zeV/k_BT$, with v_R denoting its value at current reversal. According to the Levitt theory, v_R satisfies

$$e^{v_R} = \frac{x_2 + y_2(P_Y/P_X)}{x_1 + y_1(P_Y/P_X)}, \tag{19}$$

with the permeability ratio given by:

$$P_Y/P_X = H_X/H_Y, \tag{20}$$

where

$$H_Z = L \int_0^1 D_Z^{-1}(\lambda) A_Z^{-1}(\lambda) e^{\phi_Z(\lambda) + \psi(\lambda)} d\lambda\,. \tag{21}$$

The diffusion coefficient D_2, channel cross-section A_2, intrinsic component of the electrical potential ϕ_2, and applied component of the electrical potential ψ, are all functions of the dimensionless coordinate λ along the axis of the pore. This coordinate is the displacement into the channel from the entrance at side 1, divided by the channel length L. The boundary conditions on ψ are $\psi(0) = v$ and $\psi(1) = 0$.

Consider the configuration $[x_1 \| y_2]$, with $x_1 = x_0$ and $y_2 = y_0$ chosen to give $V_R(x_1, y_2) = 0$. At zero applied potential, $\psi(\lambda) = 0$. It follows from Eqs. 19–21 that x_0 and y_0 satisfy

$$\frac{x_0}{y_0} = \frac{\int_0^1 D_X^{-1} A_X^{-1} e^{\phi_X} d^\lambda}{\int_0^1 D_Y^{-1} A_Y^{-1} e^{\phi_Y} d^\lambda}. \tag{22}$$

The same expression results if we consider the configuration $[y_1 \| x_2]$ with $y_1 = y_0$ and $x_2 = x_0$. In the simplest interpretation of the Levitt theory, the right hand side of Eq. 22 does not depend on the configuration, and the orientation independence symmetry is satisfied at $V_R = 0$. Of course, mechanisms such as asymmetrical screening of surface charges or allosteric effects could change this conclusion.

As an illustration of the violation of the orientation independence symmetry in a plausible channel model, we have analyzed the 3B2S double-occupancy permeation mechanism proposed by Ravindran et al. (1992). As shown by those authors, this model is consistent with the results of Garber's (1988) experiments on the orientation dependence of Na^+ channel permeability ratios. To account for the strong orientation dependence of the Na^+/K^+ permeability ratios found by Garber, the 3B2S model has a highly asymmetric energy profile for K^+ permeation. As a consequence, when this model is used to predict the Na^+/K^+ permeability ratios near $V_R = 0$, a violation of the orientation independence symmetry is found. We give two example symmetry plots in Fig. 2*B*. For fixed $[K^+] = 100$ mM, the violation is 2 mV or less (judged by where the symmetry plot crosses the coordinate axes). For fixed $[K^+] = 2$ M, the violation is between 5 and 7 mV. For comparison, the experimental errors for individual reversal potential measurements given by Garber range from 2 to 5 mV. If a violation of orientation independence at $V_R = 0$ could be established experimentally, this would provide significant evidence that the single-ion mechanism does not adequately describe permeation through the Na^+ channel.

This Na^+ channel example shows the importance of constructing symmetry plots over a range of fixed concentrations. A significant violation of the orientation indepen-

dence symmetry may occur only for an intermediate range of permeant ion concentrations. At sufficiently low concentrations, a 3B2S mechanism is well approximated by a single-ion model. This can be seen by comparing the state diagram for the single-ion model in the orientation $[X \| Y]$, Fig. 4*D*, with the corresponding diagram for the 3B2S model, Fig. 3*A*, when doubly occupied states are excluded. Therefore, at such low concentrations, a 3B2S mechanism would not give a significant violation of the orientation independence symmetry. This is illustrated by the Lo K example in Fig. 2*B*. Similarly, at sufficiently high concentrations (when these are attainable), a 3B2S mechanism is well approximated by a single-vacancy model. Compare the state diagram of Fig. 4*A* with that of Fig. 3*A* with the empty state and state 4 excluded. At such high concentrations, a 3B2S model would again not give a significant violation of the symmetry.

There is some evidence suggesting orientation dependence of permeability ratios in K^+ channels. Wagoner and Oxford (1987) found that P_{Rb}/P_K and P_{NH4}/P_K were orientation dependent in voltage-clamped squid axon K^+ channels. More recently, the orientation dependence of P_{Rb}/P_K has been measured in Shaker K^+ channels expressed in patch-clamped *Xenopus* oocytes (Heginbotham and MacKinnon, 1993) and an insect cell line (Pérez-Cornejo and Begenisich, 1994). Heginbotham and MacKinnon (1993) found $P_{Rb}/P_K = 0.66$ in the configuration [105 mM K^+ ‖ 95 mM Rb^+] and $P_{Rb}/P_K = 0.88$ in [105 mM Rb^+ ‖ 95 mM K^+], where the ionic species on the intracellular side is represented in the first slot. Pérez-Cornejo and Begenisich (1994) found $P_{Rb}/P_K = 0.89$ in the configuration [134 mM K^+ ‖ 122 mM Rb^+] and $P_{Rb}/P_K = 0.68$ in [110 mM Rb^+ ‖ 90 mM K^+]. Although these differences in permeability ratios are small, the results are interesting because the measurements take place at V_R values of only a few millivolts. This suggests that a violation of orientation independence, if it exists, may be measurable.

APPENDIX

A: Single Ion Models Have Orientation Independence Symmetry at $V_R = 0$

We show here that a two-site single-ion channel has the orientation independence symmetry when $V_R = 0$. Let $Z \epsilon \{X, Y\}$. a_Z denotes the second order rate constant for ion entrance from side 1, b_Z the first order rate constant for ion exit to side 2, and c_Z the first order rate constant for translocation between the ion binding sites toward side 2. a'_Z, b'_Z, and c'_Z denote the corresponding rate constants in the direction of side 1. Detailed balance requires

$$a_Z b_Z c_Z = a'_Z b'_Z c'_Z. \tag{A1}$$

Consider the state diagram for the two-site single-ion channel in the biionic configuration $[x \| y]$, Fig. 4*D*. Unidirectional currents $\vec{J}$ and $\overleftarrow{J}$ are shown. These can be evaluated as (Hill 1977):

$$\vec{J} = D^{-1}A_Y C_X \tag{A2}$$

$$= D^{-1}[b_Y c_Y + b'_Y c'_Y + b_Y b'_Y]x_1 a_X b_X c_X, \tag{A3}$$

$$\overleftarrow{J} = D^{-1}A_X C_Y \tag{A4}$$

$$= D^{-1}[b_X c_X + b'_X c'_X + b_X b'_X]y_2 a_Y b_Y c_Y\,. \tag{A5}$$

Current reverses at $V_R = 0$ when $\vec{J} = \overleftarrow{J}$, or

$$\frac{y_2}{x_1} = \frac{a_X b_X c_X[b_Y c_Y + b'_Y c'_Y + b_Y b'_Y]}{a'_Y b'_Y c'_Y[b_X c_X + b'_X c'_X + b_X b'_X]} \tag{A6}$$

Now consider the reverse configuration $[y_1 \| x_2]$. The condition for current reversal may be obtained, starting from Eq. A6, by interchanging the subscripts X and Y and replacing $x_1 \rightarrow y_1$ and $y_2 \rightarrow x_2$. The result is

$$\frac{x_2}{y_1} = \frac{a_Y b_Y c_Y[b_X c_X + b'_X c'_X + b_X b'_X]}{a'_X b'_X c'_X[b_Y c_Y + b'_Y c'_Y + b_Y b'_Y]}\,. \tag{A7}$$

Taking the reciprocal and using detailed balance, Eq. A1, we find that y_1/x_2 is equal to the expression on the right hand side of Eq. A6. If $x_1 = x_0$ and $y_2 = y_0$ satisfies the zero current condition in the configuration $[x_1 \| y_2]$, then $x_2 = x_0$ and $y_1 = y_0$ satisfies the zero current condition in the configuration $[y_1 \| x_2]$.

This argument can be immediately generalized to apply to an m-site single-ion channel. A_Y is constructed in a manner analogous to that given in the proof for m-site single-vacancy channels.

B: *m*-Site SV Models Have Orientation Independence Symmetry at $V_R = 0$

We prove here that general m-site single-vacancy models have orientation-independent reversal potentials when $V_R = 0$. For each ion species $Z \epsilon \{X, Y\}$ we use a_Z and a'_Z to denote the second order rate constants for ion entrance from the electrolyte of sides 1 or 2, respectively. b_Z and b'_Z denote the rate constants for exiting the channel to sides 2 or 1. Ion translocation into a vacant site i will be denoted $c_{Z,i}$ if the translocation is from site $i - 1$, or they will be denoted $c'_{Z,i}$ if the translocation is from site $i + 1$. The rate constants for transitions toward side 1 are primed. At thermodynamic equilibrium, no net current passes through the channel. This implies that the rate constants for each ion species must satisfy detailed balance:

$$a_Z b_Z c_{Z,2} \ldots c_{Z,m} = a'_Z b'_Z c'_{Z,1} \ldots c'_{Z,m-1}. \tag{A8}$$

Now consider a channel in the biionic configuration $[x_1 \| y_2]$; the state diagram is given in Fig. 5*A*. Assume that the electrical potential difference across the membrane is zero. There is no net current through the channel when the flux $\vec{J}$ of X ions toward side 2 is equal to the flux $\overleftarrow{J}$ of Y ions toward side 1. The flux of X ions to the right is equal to the rate of transitions clockwise around the top cycle. According to the King-Altman method (Hill, 1977) this has the form

$$\vec{J} = D^{-1}A_Y B_{YX} C_X \tag{A9}$$

C_X is the product of rate constants clockwise around the top cycle:

$$C_X = x_1 a_X b_X c_{X,2} \ldots c_{X,m}\,. \tag{A10}$$

B_{YX} is the product of rates up the bridge from the bottom cycle to the top cycle. This product is proportional to $m - 1$ factors of x_1, each corresponding to an entrance of an X ion into the channel from side 1:

$$B_{YX} = x_1^{m-1} k(-M, -M + 1) \ldots k(M - 1, M)\,. \tag{A11}$$

A_Y is the sum of products of rate constants, corresponding to trees directed out of the bottom cycle of Fig. 5*A*. Each tree corresponds to one bond that

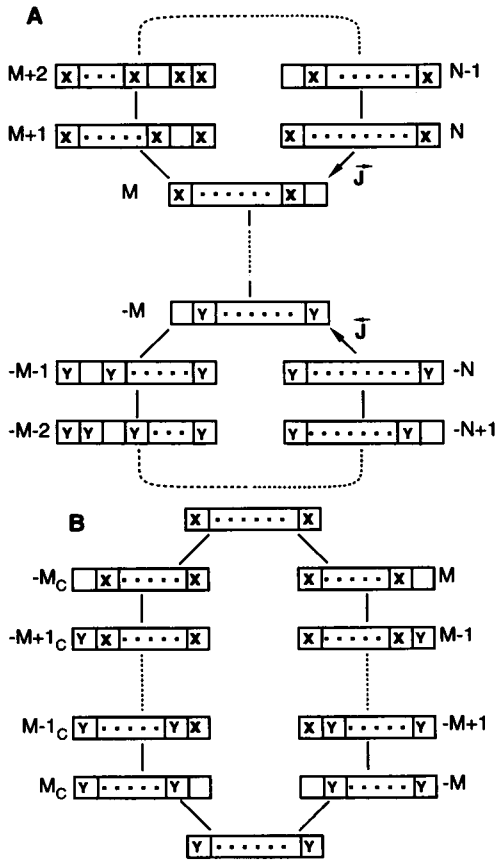

FIGURE 5 (*A*) State diagram for the *m*-site single-vacancy model in the orientation $[X \| Y]$. Dashed curves include states not shown explicitly in the diagram. (*B*) A cycle in the state diagram for the *m*-site single-vacancy model in the orientation $[X, Y \| X, Y]$. The detailed balance condition for this cycle completes the proof of orientation independence at $V_R = 0$.

is deleted between two occupancy states. A product of rate constants is then formed, each term representing a transition directed away from those occupancy states, toward the bridge.

$$A_Y = y_2 a'_Y b'_Y \sum_{k=1}^{m-1} \prod_{i=2}^{k} c_{Y,i} \prod_{j=k+1}^{m-1} c'_{Y,j} + b'_Y \prod_{i=2}^{m} c_{Y,i} + b_Y \prod_{j=2}^{m} c_{Y,j} \quad \text{(A12)}$$

Products give a factor of 1 when the initial value of the product index is greater than the final value. Multiply Eq. A12 by $a_Y^{-1} a_Y$ and use detailed balance to transform the last term. Then factor out b'_Y to get

$$A_Y = a_Y^{-1} b'_Y S_Y(y_2) \quad \text{(A13)}$$

where

$$S_Y(y_2) = y_2 a_Y a'_Y \sum_{k=1}^{m-1} \prod_{i=2}^{k} c_{Y,i} \prod_{j=k+1}^{m-1} c'_{Y,j} + a_Y \prod_{i=2}^{m} c_{Y,i} + a'_Y \prod_{j=1}^{m-1} c'_{Y,j}. \quad \text{(A14)}$$

Similarly, we calculate the expression for $\tilde{J}$.

$$\tilde{J} = D^{-1} A_X B_{XY} C_Y, \quad \text{(A15)}$$

$$C_Y = y_2 a'_Y b'_Y c'_{Y,1} \ldots c'_{Y,m-1}, \quad \text{(A16)}$$

$$B_{XY} = y_2^{m-1} k(M, M-1) \ldots k(-M+1, -M), \quad \text{(A17)}$$

$$A_X = (a'_X)^{-1} b_X S_X(x_i), \quad \text{(A18)}$$

where

$$S_X(x_1) = x_1 a_X a'_X \sum_{k=1}^{m-1} \prod_{i=2}^{k} c_{X,i} \prod_{j=k+1}^{m-1} c'_{X,j} + a_X \prod_{i=2}^{m} c_{X,i} + a'_X \prod_{j=1}^{m-1} c'_{X,j}. \quad \text{(A19)}$$

These formulas can be obtained from Eqs. A9–A14 by interchanging *X* and *Y* subscripts, primes and nonprimes, and the concentrations x_1 and y_2. The product of rate constants up the bridge is replaced also with the product down the bridge.

The current through the channel in the biionic configuration $[x_1 \| y_2]$ reverses when $\tilde{J} = \bar{J}$, or:

$$\frac{x_1^m a_X b_X c_{X,2} \ldots c_{X,m} S_Y(y_2)}{y_2^m a'_Y b'_Y c'_{Y,1} \ldots c'_{Y,m} S_X(x_1)} = \frac{a_Y b_X k(M, M-1) \ldots k(-M+1, -M)}{a'_X b'_Y k(-M, -M+1) \ldots k(M-1, M)} \quad \text{(A20)}$$

We now write the equation for the reverse configuration $[y_1 \| x_2]$. The complementary state diagram is related to Fig. 5*A* in the same way as Fig. 4*B* is related to Fig. 4*A*. Interchange the subscripts *X* and *Y*, replace $x_1 \rightarrow y_2$ and $y_1 \rightarrow x_2$, and replace references to states along the bridge by references to complementary states to obtain

$$\frac{y_1^m a_Y b_Y c_{Y,2} \ldots c_{Y,m} S_X(x_Z)}{x_2^m a'_X b'_X c'_{X,1} \ldots c'_{X,m-1} S_Y(y_1)} = \frac{a_X b_Y k(M_C, M-1_C) \ldots k(-M+1_C, -M_C)}{a'_Y b'_X k(-M_C, -M+1_C) \ldots k(M-1_C, M_C)}. \quad \text{(A21)}$$

Now take the reciprocal of this equation and use detailed balance to interchange primes on the left.

$$\frac{x_2^m a_X b_X c_{X,2} \ldots c_{X,m} S_Y(y_1)}{y_1^m a'_Y b'_Y c'_{Y,1} \ldots c'_{Y,m-1} S_X(x_Z)} = \frac{a'_Y b'_X k(-M_C, -M+1_C) \ldots k(M-1_C, M_C)}{a_X b_Y k(M_C, M-1_C) \ldots k(-M+1_C, -M_C)}. \quad \text{(A22)}$$

Equations A20 and A22 have the respective forms of Eq. 17, where *f* is again the same function on the left side of both equations. Consider the cycle in the state diagram for the *m*-site single-vacancy model in the configuration $[x_0, y_0 \| x_0, y_0]$ shown in Fig. 5*B*. This system is in equilibrium when the transmembrane potential is zero. Writing out the detailed balance relationship for the cycle leads immediately to $K = K_C$. It follows that Eqs. A20 and A22 are the same and therefore have the same solutions. We show in Appendix D that, given $y_2 = y_1 = y_0 > 0$, there is a unique $x_1 = x_2 = x_0 > 0$ satisfying these equations.

C: Orientation Independence Symmetry of the Shaking-Stack Model

Shaking-stack model permeability ratios are also independent of orientation when $V_R = 0$. This model was proposed for the high conductance Ca^{2+}-activated K^+ channel, based on several experimental studies, in particular, those of Neyton and Miller (1988a,b). The physical idea is that the selective region of the channel is occupied by a stack of m or $m - 1$ ions, which are associated with m high affinity ion binding sites. Ions can enter or exit the stack only at its ends, and the stack can also translocate between two possible sets of $m - 1$ binding sites (shifting a vacancy from binding site 1 to binding sites m, or vice versa). This model also has the orientation independence symmetry when $V_R = 0$; the proof is a hybrid of the two-site and m-site single-vacancy arguments.

The m-site shaking stack model has only ion entry, stack translocation, and ion exit steps. Stack translocation plays the role corresponding to ion translocation in the two-site model. Similar to Fig. 4, *A* and *B*, the biionic state diagrams have cycles of only three states at either end of a bridge. However, the bridge has more states than that of the two-site model; it can be obtained from the bridge for the m-site single-vacancy diagram by omitting states with interior vacancies. The unidirectional current $\tilde{J}$ in the configuration $[x_1 \| y_2]$ is given by expressions like Eqs. 6–9, except that B_{YX} has more terms and is proportional to x_1^{m-1}. In the same way, the unidirectional current $\tilde{J}$ is given by expressions similar to Eqs. 10–13. The condition for current reversal and its comparison with that of the reverse configuration is completely analogous to the two-site argument. Given $y_0 > 0$, current reversal is obtained for a unique $x_0 > 0$, as shown in the next section.

D: Uniqueness of Concentration Giving Current Reversal

We show here that, for a general m-site single-vacancy or shaking-stack model, and given a fixed $y_2 = y > 0$, the current reversal equation $\tilde{J}(x_1, y_2) = \tilde{J}(x_1, y_2)$ has only a single positive root $x_1 = x > 0$. Consider Eqs. A9 and A15 or the corresponding equations for the shaking-stack model. The equation for current reversal, $\tilde{J} = \tilde{J}$, has the form

$$Ax^m + Bx^m y = Cy^m + Dxy^m, \qquad \text{(A23)}$$

where A, B, C, and D are positive combinations of rate constants. Now fix $y = y_0 > 0$ and rewrite Eq. A23 as

$$f(x) = xp(x) = \gamma, \qquad \text{(A24)}$$

with $p(x) = \alpha x^{m-1} - \beta$ and α, β, and γ all positive. The real roots of Eq. A24 correspond to the curve $z = f(x)$ intersecting the horizontal line $z = \gamma$ in the xz plane. $p(x)$ has a unique positive root r. For $0 < x < r$, $f(x) < 0$. For $x > r$, x and $p(x)$ increase monotonically and without bound and, therefore, so does $f(x)$. It follows that there is a unique positive root $x = x_0$ such that $f(x_0) = \gamma$.

M.F.S. thanks Roderick MacKinnon for original discussions that motivated a close study of the symmetry properties of the single-vacancy reversal potential. He is grateful to Christopher Miller for referring us to the work of Sarah Garber, and for conversations regarding aspects of this work. We also thank Robert Guy for mechanistic interpretations of his molecular modeling studies.

This work was supported in part by National Science Foundation grant MCB 94–04430.

REFERENCES

Begenisich, T. B., and M. D. Cahalan. 1980. Sodium channel permeation in squid axons. I. Reversal potential experiments. *J. Physiol.* 307:217–242.

Bek, S., and E. Jakobsson. 1994. Brownian dynamics study of a multiply occupied cation channel: application to understanding permeation in potassium channels. *Biophys. J.* 66:1028–1038.

Clay, J. R. 1991. A paradox concerning ion permeation of the delayed rectifier potassium ion channel in squid giant axons. *J. Physiol.* 444:499–511.

Cooper, K. E., P. Y. Gates, and R. S. Eisenberg. 1988. Diffusion theory and discrete rate constants in ion permeation. *J. Membr. Biol.* 106:95–105.

Cooper, K., E. Jakobsson, and P. Wolynes. 1985. The theory of ion transport through membrane channels. *Prog. Biophys. Mol. Biol.* 46:51–96.

Dani, J. A., and D. G. Levitt. 1990. Diffusion and kinetic approaches to describe permeation in ionic channels. *J. Theor. Biol.* 146:289–301.

Eisenman, G., R. Latorre, and C. Miller. 1986. Multi-ion conduction and selectivity in the high-conductance Ca^{+} $^{+}$-activated K^+ channel from skeletal muscle. *Biophys. J.* 50:1025–1034.

Garber, S. S. 1988. Symmetry and asymmetry of permeation through toxin-modified Na^+ channels. *Biophys. J.* 54:767–776.

Glasstone, S., K. J. Laidler, and H. Eyring. 1941. The Theory of Rate Processes. McGraw-Hill, New York. 611 pp.

Guy, H. R., and S. R. Durrell. 1994. Using sequence homology to analyze the structure and function of voltage-gated ion channel proteins. *In* Molecular Evolution of Physiological Processes. C. M. Fambrough, editor. The Rockefeller University Press, New York. 197–212.

Heginbotham, L., Z. Lu, T. Abramson, and R. MacKinnon. 1994. Mutations in the K^+ channel signature sequence. *Biophys. J.* 66:1061–1067.

Heginbotham, L., and R. MacKinnon. 1993. Conduction properties of cloned *Shaker* K^+ channels. *Biophys. J.* 65:2089–2096.

Hill, T. L. 1977. Free Energy Transduction in Biology. Academic Press, New York. 229 pp.

Hille, B. 1992. Ionic Channels of Excitable Membranes, 2nd ed. Sinauer Assoc., Sunderland, MA. 280.

Hodgkin, A. L., and R. D. Keynes. 1955. The potassium permeability of a giant nerve fiber. *J. Physiol. (Lond.).* 128:61–88.

Kohler, H.-H., and K. Heckmann. 1979. Unidirectional fluxes in saturated single file pores of biological and artificial membranes. I. Pores containing no more than one vacancy. *J. Theor. Biol.* 79:381–401.

Levitt, D. G. 1984. Kinetics of movement in narrow channels. *Curr. Top. Membr. Transp.* 21:182–197.

Levitt, D. G. 1986. Interpretation of biological ion channel flux data: reaction rate versus continuum theory. *Annu. Rev. Biophys. Biophys. Chem.* 15:29–57.

Lu Z., and R. MacKinnon. 1994. A conductance maximum observed in an inward-rectifier potassium channel. *J. Gen. Physiol.* 104:477–486.

MacKinnon R., R. Latorre, and C. Miller. 1989. Role of surface electrostatics in the operation of a high-conductance Ca^{2+}-activated K^+ channel. *Biochemistry.* 28:8092.

Naranjo D., and R. Latorre. 1993. Ion conduction substates of the batrachotoxin-modified Na^+ channel from toad skeletal muscle. *Biophys. J.* 64:1038–1050.

Neyton, J., and C. Miller. 1988a. Potassium blocks barium permeation through a calcium-activated potassium channel. *J. Gen. Physiol.* 92:549–567.

Neyton, J., and C. Miller. 1988b. Discrete Ba^{2+} block as a probe of ion occupancy and pore structure in the high-conductance Ca^{2+}-activated K^+ channel. *J. Gen. Physiol.* 92:569–586.

Pérez-Cornejo, P., and T. Begenisich. 1994. The multi-ion nature of the pore in *Shaker* K^+ channels. *Biophys. J.* 66:1929–1938.

Ravindran A., H. Kwiecinski, O. Alvarez, G. Eisenman, and E. Moczydlowski. 1992. Modeling ion permeation through batrachotoxin-modified Na^+ channels from rat skeletal muscle with a multi-ion pore. *Biophys. J.* 61:494–508.

Schumaker M. F. 1992. Shaking stack model of ion conduction through the Ca^{2+}-activated K^+ channel. *Biophys. J.* 63:1032–1044.

Schumaker M. F., and R. MacKinnon. 1990. A simple model for multi-ion permeation. *Biophys. J.* 58:975–984.

Vestergaard-Bogind, B., P. Stampe, and P. Christophersen. 1985. Single-file diffusion through the Ca^{2+}-activated K^+ channel of human red blood cells. *J. Membr. Biol.* 88:67–75.

Wagoner, K., and G. S. Oxford. 1987. Cation permeation through the voltage-dependent potassium channel in the squid axon. *J. Gen. Physiol.* 90:261–290.